Cellular and Molecular Bioengineering, Vol. 10, No. 5, October 2017 *(© 2017)* pp. 463–481
DOI: 10.1007/s12195-017-0498-3

Chemoprotection Across the Tumor Border: Cancer Cell Response to Doxorubicin Depends on Stromal Fibroblast Ratios and Interstitial Therapeutic Transport

DANIEL K. LOGSDON,[1] GARRETT F. BEEGHLY,[1] and JENNIFER M. MUNSON[1,2]

[1]Department of Biomedical Engineering, University of Virginia School of Medicine, Charlottesville, VA 22908, USA; and [2]Department of Biomedical Engineering and Mechanics, Virginia Tech, Kelly Hall, 325 Stanger Street, Blacksburg, VA 24061, USA

(Received 10 February 2017; accepted 20 July 2017; published online 2 August 2017)

Associate Editor Michael King oversaw the review of this article.

Abstract

Introduction—Increasing evidence suggests that the tumor microenvironment reduces therapeutic delivery and may lead to chemotherapeutic resistance. At tumor borders, drug is convectively transported across a unique microenvironment composed of inverse gradients of stromal and tumor cells. These regions are particularly important to overall survival, as they are often missed through surgical intervention and contain many invading cells, often responsible for metastatic spread. An understanding of how cells in this tumor-border region respond to chemotherapy could begin to elucidate the role of transport and intercellular interactions in relation to chemoresistance. Here we examine the contribution of drug transport and stromal fibroblasts to breast cancer response to doxorubicin using *in silico* and *in vitro* models of the tumor-stroma interface.

Methods—2D culture systems were utilized to determine the effects of modulated ratios of fibroblasts and cancer cells on overall cancer cell viability. A homogenous breast mimetic *in vitro* 3D collagen I-based hydrogel system, with drug delivered *via* pressure driven flow (0.5 μm/s), was developed to determine the effects of transport and fibroblasts on doxorubicin treatment efficacy. Using a novel layered tumor bulk-to-stroma transition *in vitro* 3D hydrogel model, ratios of MDA-MB-231s and fibroblasts were seeded in successive layers creating cellular gradients, yielding insight into region specific cancer cell viability at the tumor border. *In silico* models, utilizing concentration profiles developed in COMSOL Multiphysics, were optimized for time dependent viability prediction and confirmation of *in vitro* findings.

Results—In general, the addition of fibroblasts increased viability of cancer cells exposed to doxorubicin, indicating a protective effect of co-culture. More specifically, however, modulating ratios of cancer cells (MDA-MB-231):fibroblasts in 2D co-cultures, to mimic the tumor-stroma transition, resulted in a linear decrease in cancer cell viability from 77% (4:1) to 44% (1:4). Similar trends were seen in the

Address correspondence to Jennifer M. Munson, Department of Biomedical Engineering and Mechanics, Virginia Tech, Kelly Hall, 325 Stanger Street, Blacksburg, VA 24061, USA. Electronic mail: munsonj@vt.edu

Jennifer M. Munson, Ph.D. is an Assistant Professor of Biomedical Engineering at the University of Virginia. Dr. Munson received her Bachelor of Science in Chemical Engineering and Neuroscience from Tulane University in 2006. She worked at Genentech in Process Engineering before pursuing graduate study at Georgia Tech with Ravi Bellamkonda, Ph.D. Supported by a National Science Foundation Graduate Research Award, she developed liposomal nanocarriers to deliver a novel anti-invasive therapeutic to glioblastoma. During her Ph.D. she was awarded a Fulbright Fellowship to Switzerland to pursue independent study on the glioma microenvironment at L'École Polytechnique Fédérale de Lausanne with Melody Swartz, Ph.D. After completing her Ph.D. in 2011, she returned to Switzerland as a Whitaker Scholar for postdoctoral training on the breast cancer microenvironment, focusing on changes that alter interstitial transport. Dr. Munson began her faculty career at the University of Virginia in 2014 and moved to Virginia Tech to the Department of Biomedical Engineering and Mechanics in 2017, pursuing research interests related to the cancer microenvironment, drug delivery, and transport in brain and breast cancers. Her work includes the development of tissue engineered systems for the study of interstitial flow and tissue transport as well as translation of these systems for patient-specific drug screening. She was awarded the Rita Schaffer Young Investigator Award by the Biomedical Engineering Society in 2016.

This article is part of the 2017 CMBE Young Innovators special issue.

breast-mimetic *in vitro* 3D collagen I-based homogenous hydrogel system. Our *in vitro* and *in silico* tumor border models indicate that MDA-MB-231s at the top of the gel, indicative of the tumor bulk, receive the greatest concentration of drug for the longest time, yet cellular death is lowest in this region. This trend is reversed for MDA-MB-231s alone.
Conclusion—Together, our data indicate that fibroblasts are chemoprotective at lower density, resulting in less tumor death in regions of higher chemotherapy concentration. Additionally, chemotherapeutic agent transport properties can modulate this effect.

Keywords—Tumor microenvironment, Drug delivery, Doxorubicin, Fibroblasts, Breast cancer, Interstitial flow, 3D cell culture.

ABBREVIATIONS

MDA-MB-231	Human breast triple negative adenocarcinoma cell line (luminal)
HCC38	Human breast triple negative invasive ductal carcinoma cell line (luminal)
MCF7	Human breast ER+/PR+ adenocarcinoma cell line (basal)
HDF	Human dermal fibroblast
TC	Tumor cell
Fb	Fibroblast
ABM	Agent-based model
TME	Tumor microenvironment
TSTM	Tumor to stroma transition model
IFP	Interstitial fluid pressure
DOX	Doxorubicin

INTRODUCTION

Chemotherapy is a near-ubiquitous treatment approach for multiple forms of solid tumor cancers. Though it works in many cases, chemotherapy often fails, resulting in poor prognosis across multiple forms of the disease. Doxorubicin (DOX) is a commonly used chemotherapy against multiple cancers including breast, bladder, ovarian, and lung, alone or in concert with other treatments.[3] Doxorubicin is a common chemotherapeutic delivered prior to, or after surgery in cases of the deadliest form of breast cancer, triple negative. In addition to its clinical relevance, as a drug with well-understood pharmacokinetics, doxorubicin provides an optimal model drug for probing dynamics of chemotherapeutic treatment.[3,54,64]

Systemic chemotherapeutic delivery has been limited, first and foremost, by transport restrictions to and within tumors.[28] Specifically, the tumor microenvironment (TME), defined as the tumor cells, tumor-associated cells, extracellular matrix, and biomechanical forces,[60,71] that interact in and around the tumor, provides two distinct barriers to drug delivery. Firstly, delivery of chemotherapeutic agents to the tumor bulk from the circulation is attenuated by interstitial fluid pressure, which is elevated in tumors.[21] This pressure can limit the transvascular movement of small molecule drugs into the interstitial spaces leading to retention of therapy, particularly larger molecules, near the tumor-associated blood vessels. Drug that penetrates into the interstitial tumor space is subject to a number of further constraints, which limit the transport through the tissue. Limited transport of therapeutic agents results from matrix deposition and crosslinking by cancer associated fibroblasts, uptake by therapeutics by stromal cells, and reduced overall void space due to unrestricted cell growth.[60]

This limited drug distribution is thought to particularly reduce therapeutic access to invading cancer cells at the tumor border. These cells are especially deadly as they are thought to be responsible for subsequent metastasis of cancers, which is a leading cause of death. Interestingly, at these border regions of the tumors, where cells are invading, there is increased interstitial fluid flow. The higher interstitial fluid pressure in the tumor bulk relative to the normal pressure in the surrounding stroma yields an efflux of fluid from the tumor to the surrounding tissue.[43] These forces are known to alter cellular invasion, promoting movement towards draining lymphatics.[45,63] However, the interaction of these particular forces with chemotherapeutic transport and delivery is not explored in the context of this complex transitional microenvironment.

Secondly, intercellular interactions in the tumor microenvironment also contribute to reduced therapeutic response. Several TME-mediated factors have been implicated in the development of chemotherapy resistance within solid tumors.[67] These factors include hypoxia,[57] reduced pH,[52] nutrient deprivation,[35] adhesion-mediated resistance,[20,56] and drug gradient formation.[32] However, cancer-stromal interactions, specifically between cancer cells and fibroblasts in the breast cancer context, appear to be a dominating factor in acquired chemotherapy resistance.[49] Cancer associated fibroblasts secrete pro-survival factors that limit cancer cell apoptosis and could act to protect cancer cells from chemotherapeutic effects.[33] In the context of neoadjuvant breast cancer therapy, the presence of cancer associated fibroblasts signatures has been directly implicated in poorer survival outcomes,[11]and targeted therapy against these stromal cells has been shown to improve intratumoral uptake of doxorubicin within *in vivo* murine models.[36]

In relation to these barriers to chemotherapy response, the tumor border is a unique environment, as stromal interactions, chemotherapy and cytokine gradients, and interstitial flow are all present in this region. Interstitial fluid velocity and pressure are the greatest at the tumor border,[27] thus mediating convection-driven chemotherapy transport through this region.[25] Additionally, gradients of doxorubicin have been observed at the breast tumor border *in vivo*,[32] providing a potential for adaptive chemotherapy resistance. Finally, cancer cell propinquity to stromal fibroblasts, coupled with zones of cellular transition[14] from the tumor to the surrounding stroma, yields stromal heterogeneity. At the tumor border, the tissue transitions from regions of very few fibroblasts in the tumor bulk to regions of very few cancer cells relative to stromal cells; therefore, this transition region is defined by cellular gradients, which could mediate further cancer cell insensitivity to chemotherapy due to fibroblast interactions. Collectively, this distinct environment couples several TME-specific factors that could lead to chemotherapy resistance and decreased patient survival.

Due to the complexity of this region, robust *in vitro* and *in silico* models are necessary to probe the effects of therapy coupled with interstitial flow. *In silico* research methodologies provide a supplementary platform that can expand the numbers of outcomes and test conditions for complex biological phenomena.[7,74] Agent-based models (ABMs) are particularly suited for biological applications, as they can predict and describe both spatial and temporal biological interactions and characterize emergent behaviors.[39,69] To date, these types of models have not been applied to the tumor-stroma interface, though they have been used to model cancer cell growth,[73] progression,[30] and angiogenesis.[48] *In vitro*, organoids and similar micropatterned multicellular islands have been employed to characterize the tumor stromal interface.[40,59] While these models resolve this interface, they do not inherently incorporate extracellular matrix (ECM) components,[13] which are essential for characterizing drug distributions in tissues.[15] Most commonly, micropatterning is confined to 2D models,[31] however, drug response has been shown to differ in 2D and 3D contexts.[37,75] Though micropatterned 3D systems are possible, they are limited by the complex fabrication process.[65] Finally, many of these systems model the tumor border, however, they do not yet account for interstitial flow,[4,9,34] which has been shown to drive therapy distribution and cellular responses in this region.[45] Thus, this is a significant limitation in current engineered microtissues and tumor spheroids.

3D Collagen hydrogels with homogeneously distributed cells, an alternative to micropatterning, have been utilized to model multiple types of cancer in the context of the tumor microenvironment.[43] These models can incorporate ECM proteins and pressure driven flow,[61] thus replicating biophysical parameters inherent to *in vivo* tumors and providing a culture context that is more replicative of real tissues than 2D culture systems.[17] However, traditional hydrogel models do not resolve the spatial perspective inherent to the tumor border, as cells in these models are indiscriminately mixed.[59] Therefore, the common hydrogel paradigm must be altered in order to characterize the tumor border region and capture the distribution of cellular gradients that arise as the cancer transitions to the surrounding stroma.

Here, we establish *in vitro* and *in silico* models that elucidate the effects of fluid and solute transport, cellular heterogeneity, and fibroblast interactions on breast cancer viability following doxorubicin treatment. This work incorporates two luminal triple negative cell lines (MDA-MB-231, HCC38) and one basal ER + /PR + cell line (MCF7).[64] Our study utilizes a novel 3D *in vitro* tumor bulk to stroma transition model (TSTM) with physiologically-relevant interstitial flow, as well as concurrent 2D culture systems, to predict the regional variations in viability that occur within the microenvironment at the tumor border. This 3D hydrogel model incorporates successive layering of gels with different ratios of fibroblasts and cancer cells, yielding a vertically patterned tissue resembling the tumor border. Additionally, *in silico* methodologies predict the dominant fluid dynamic properties that influence doxorubicin treatment efficacy within the tumor border transitional region. Together our data provide evidence of a unique fibroblast protective effect, which yields varied resistance to chemotherapy in a cancer to fibroblast ratiometric dependent manner. This effect is sustained in several experimental models and three separate cell lines. These findings illuminate the importance of regional TME heterogeneity in selecting for viable populations that could be impacting breast cancer progression.

MATERIALS AND METHODS

Cell Culture

MDA-MB-231 human breast adenocarcinoma (tumor cells: TCs) and human dermal fibroblasts (Fibroblasts: Fbs) were obtained from the American Type Culture Collection (ATCC). MCF7 and HCC38 cell lines were obtained from ATCC. HDFs, MCF7, and MDA-MB-231 cell types were cultured in Dulbecco's modified Eagle's medium (DMEM, Gibco), supplemented with 10% fetal bovine serum (FBS, Seradigm). HCC38 cell types were cultured in Roswell Park Memorial Institute medium (RPMI, Gibco), supplemented with 10% fetal bovine serum (FBS, Seradigm). Cells were passaged weekly and grown at 37 °C in a

sterile incubator (5% CO_2 and 95% oxygen) in gamma irradiated tissue culture treated flasks.

Two-Dimensional (2D) Conditioned Media Assay

Fb-conditioned media was created by incubating fibroblasts in cell culture flasks with full (DMEM + 10% FBS) media for 24 h. Control media was collected from a second flask incubated simultaneously, in the absence of cells. MDA-MB-231 cells were seeded into a 48 well tissue culture treated plate at a density of 20,000 cells per well into either Fb-conditioned or unconditioned media. After 24 h, the media was replaced with 10 μM of doxorubicin HCl (Fisher Scientific) in serum free media. TC percent live and doxorubicin accumulation were determined as described.

Two-Dimensional (2D) Hanging Well Co-culture Assay

MDA-MB-231 cells were seeded into a 24 well tissue culture companion plate for hanging cell culture inserts (VWR International) at a density of 40,000 cells per well. HDFs were seeded into hanging culture inserts (VWR international), with 1.0 μm membrane pore size, at a density of 10,000 cells per insert. For the control condition, HDF seeding was neglected. Cells were grown in serum free DMEM for 24 h. Prior to introduction of chemotherapy, the cell culture insert was removed for the conditioned experimental group. Doxorubicin was introduced, to bring the final concentration to 10 μM. TC percent live and doxorubicin accumulation were determined as described.

Two-Dimensional (2D) Ratiometric Co-culture Assay

HDFs and Cell Tracker (ThermoFisher) deep red labelled MDA-MB-231 cells were introduced into the same well of a 48 well tissue culture treated cell culture plate at varied ratios of cancer cells to fibroblasts (4:1, 2:1, 1:1, 1:2, 1:4). Here, the total cell density was held constant at 30,000 cells, and cell numbers were varied internally. For example, a ratio of 4:1 had 24,000 cancer cells and 6000 fibroblasts, while a ratio of 2:1 had 20,000 cancer cells and 10,000 fibroblasts. Control conditions were seeded at cancer cell densities comparable to experimental conditions, however, fibroblasts were not introduced. The cells were incubated for 24 h at 37 °C, followed by introduction of 10 μM doxorubicin HCL diluted in serum free DMEM.

Two-Dimensional (2D) Live/Dead Analysis

Following 6 h of doxorubicin treatment and subsequent 24 h incubation in serum free DMEM, cells were incubated with NucBlue live cell stain (Life Technologies) and NucGreen Dead 488 cell stain (Life Technologies) in serum free DMEM for 20 min at room temperature. Each experimental well was imaged using fluorescence microscopy (EVOS FL). Live and dead cells were counted using the ImageJ cell counter plugin (NIH). For co-culture assays, cancer cells were identified by the presence of the CellTracker Deep Red dye prior to assessment for live/dead. For all assays, five images were taken per experimental technical replicate (n = 3 per experiment) and averaged for statistical analysis.

Doxorubicin Accumulation Analysis

For doxorubicin accumulation experiments, the cells were trypsinized (0.25% trypsin, Gibco) at 2 h time points (at 6 h post doxorubicin introduction for the 2D hanging well experiments), centrifuged at 2000 rpm for 2 min, and subsequently lysed with RIPA Buffer (Thermo Scientific) for 15 min on ice. Cellular lysate fluorescence intensity was determined using a fluorescent plate reader (Omega FLUOstar) at 495 nm excitation and 590 nm emission. Fluorescence intensity was compared to a doxorubicin standard curve for concentration determination.

Three-Dimensional (3D) Homogenous In vitro Interstitial Flow Model

50ul of rat tail collagen I (Corning) and basement membrane extract (Trevigen) (1.8 mg/mL Collagen, 0.5 mg/mL BME), containing cell tracker deep red dye (ThermoFisher) labelled MDA-MB-231 cells and HDFs at varied ratios (TC alone, 4:1, 1:1, 1:4) of cancer cells to fibroblasts, was added into a 96-well tissue culture insert (Corning). Total cell density in the gels was 100,000 total cells/mL. Hydrogels were crosslinked at 37 °C for 30 min. Afterward, the gels were rehydrated with a drop of serum free media and placed in an incubator for 3 h, to allow for cell adhesion within the matrix. After 3 h, serum free DMEM was added to the bottom compartment of the insert and either serum free DMEM (control condition) or 10 μM doxorubicin diluted in basal DMEM was added onto the top of the gel. Gravity driven flow (~0.5 μm/s) was introduced for 18 h, at which point the media was removed, and the gels were flushed with basal media for a comparable amount of time. The basal media was replaced with NucBlue live cell stain (Life Technologies) and NucGreen Dead 488 cell stain (Life Technologies) in serum free DMEM and incubated for 1 h at 37 °C.

The gels were removed from the inserts and imaged using fluorescent microscopy (EVOS FL). Five images were taken per experimental technical replicate and

averaged for statistical analysis. Dead cancer cells were determined by colocalization of blue, deep red, and green fluorescent markers.

Three Dimensional (3D) In vitro Tumor to Stroma Transition Hydrogel Model

Five separate solutions of rat tail collagen I (Corning) and basement membrane extract (Trevigen) (1.8 mg/mL collagen, 0.5 mg/mL BME) containing cell tracker deep red dye (Thermo Fisher) labelled MDA-MB-231 cells and HDFs at varied ratios (4:1, 2:1, 1:1, 1:2, 1:4) of cancer cells to fibroblasts were created. Each solution had a total cell density of 100,000 total cells/mL. 50 μL of successive ratios starting with 1:4 were introduced into a tissue culture insert (Corning) with 20 min of crosslinking at 37 °C between the addition of each new layer. After the final layer was added, the entire gel was crosslinked at 37 °C for 45 min. For the single culture layered gels, the same procedure was followed, however, cancer cells were seeded in the gels in the absence of HDFs at densities comparable to the experimental MDA-MB-231 densities.

Basal media was introduced into the bottom of the cell culture insert. Either basal media or 10 μM doxorubicin solution was added to the top of the hydrogel. Fluid flowed through the gel (~0.5 μm/s) for 18 h. The media was removed and the gels were flushed with basal media for 18 h. Live/dead fixable green dye (Life Technologies) in PBS was flushed through the gel for 1 h. Afterward, the gels were fixed with 4% paraformaldehyde for 18 h at 4 °C. The hydrogels were removed from the inserts and stained with DAPI diluted in PBS on a shaker for 1 h. Gels were imaged using confocal fluorescent imaging (Zeiss 700). Z-stacks were developed with 25 slices through the gel. Dead cancer cells were determined by colocalization of green, deep red, and blue fluorescent markers. The dead cells in five successive slices were averaged for each technical replicate.

For imaging of the gel prior to introduction of flow, the cancer cells in the top, middle, and bottom layer were labelled with cell tracker deep red (Thermo Fisher), while all other cancer cells were labelled with cell tracker green (Thermo Fisher). The gels were immediately fixed with 4% paraformaldehyde at 4 °C for 18 h, following crosslinking. The gels were removed from the inserts and stained with DAPI diluted in PBS on a shaker for 1 h. Gels were imaged using confocal fluorescent imaging (Zeiss LSM 700). Z-stacks were developed with 200 separate slices.

Agent-Based Model Construction

COMSOL time-dependent convection diffusion concentration gradients (COMSOL Multiphysics 5.1) were developed using Darcy's law of fluid flow coupled with simple diffusion dynamics, representative of doxorubicin transport within *in vitro* breast mimetic collagen hydrogel/BME hydrogels[53] (Supplemental Methods). Physical model parameters were determined from experimental methods and literature values (Table 1). Concentration profiles were outputted as text files for use in agent-based model (ABM) simulations.

The agent-based model (ABM) was constructed using the Repast Java framework and the Relogo Java package. A 2D coordinate grid of 64 × 64 patches was initiated to represent a 4.0 mm × 3.5 mm finite slice of experimental gel.[30] For homogenous gel simulations, the total number of cells was 2800, and the fibroblasts and/or cancer cells were spawned randomly within the gel at the user specified ratios. For the layered tumor transition model, the grid space was split into 5 equivalent segments (Fig. S1C). Fibroblasts and cancer

TABLE 1. Comsol modeling parameters.

Parameter	Symbol	Value	Source
Permeability	K	3.19 e^{-14} (m^2)	Experimental
Porosity	ε_p	0.997 (dimensionless)	53
Diffusion coefficient	D	6 e^{-11} (m^2/s)	53
Time dependent fluid volume	V	$V = \beta_1 + \left(\frac{\beta_2-\beta_1}{1+\frac{\beta_3}{t}}\right)^{\beta_4}$ (μL)	Experimental
Curve fitting parameter	β_1	37.94 (μL)	Experimental
Curve fitting parameter	β_2	84.56 (μL)	Experimental
Curve fitting parameter	β_3	1.09 (h)	Experimental
Curve fitting parameter	β_4	4.00 (dimensionless)	Experimental
Fluid density	ρ	993 (kg/m^2)	Known
Dynamic viscosity	μ	6.91 e^{-4} (Pa s)	Known
Stromal uptake rate	R_f	2.75 e^{-7} (mol/m^3 s)	Experimental

TABLE 2. Agent-based model equations and parameters.

Parameter	Cell type	Equation	Units	Bounds/variables
2D IC50 percent live	MDAMB-231	$\text{plive} = \beta_{M1} + \left(\frac{\beta_{M2} - \beta_{M1}}{1 + \frac{\beta_{M3}}{\text{dose}}}\right)^{\beta_{M4}}$	%	$\beta_{M1} = 78.11\%$ $\beta_{M2} = -0.48\%$ β_{M3} = 3.66 μM $\beta_{M4} = 1.09$ (dimensionless)
2D cellular density dependent percent live	MDAMB-231	plive = 0.0003 × density + 34.484 plive = 41.68 plive = 36.28	%	6000 ≤ Density ≤ 24,000 Density > 24,000 Density < 6000
2D 231/HDF ratio dependent percent live	MDAMB-231	$\text{plive} = -2.50 \times \text{ratio}^2 + 18.77 \times \text{ratio} + 41.054$ plive = 76.38 plive = 43.71	%	0.25 Ratio ≤ 4 Ratio > 4 Ratio < 0.25
2D IC50 percent live	HDF	$\text{plive} = \beta_{H1} + \left(\frac{\beta_{H2} - \beta_{H1}}{1 + \frac{\beta_{H3}}{\text{dose}}}\right)^{\beta_{H4}}$	%	$\beta_{H1} = 74.07\%$ $\beta_{H2} = 0.04\%$ β_{H3} = 2.105 μM $\beta_{H4} = 1.01$ (dimensionless)
2D cellular density dependent percent live	HDF	plive = − 0.0011 × density + 60.88 plive = 54.28 plive = 34.48	%	6000 ≤ Density ≤ 24,000 Density > 24,000 Density < 6000
2D 231/HDF ratio dependent percent live	HDF	$\text{plive} = -4.30 \times \text{ratio}^2 + 29.75 \times \text{ratio} + 15.82$ plive = 66.02 plive = 22.99	%	0.25 ≤ Ratio ≤ 4 Ratio > 4 Ratio < 0.25

cells were spawned randomly within the sections at user specified ratios for a total cell number of 2800. For the single culture tumor transition model, cancer cells were spawned within segments at densities comparable to experimental conditions. The total cell number was 1400 (Fig. S1B).

Each tic of the scheduling method corresponded to 1 min. At each subsequent tic of the scheduling method (Fig. S2A), a new concentration profile was parsed and concentration values were stored in appropriate patches. The patches passed these values to corresponding cell(s) located on the patches (Fig. S2B). The average concentration encountered by the cells was updated based on the stored value. At specified time intervals, the expected live percentage, based on EC50 curves and the average concentration encountered by the cells, was determined. This value was scaled to account for cellular density (Table 2). If the modeling condition accounted for both fibroblast and cancer cells, the expected live percentage was scaled to account for the fibroblast protective effect based on the ratio of cancer cells to fibroblasts. The cells were removed or kept in the simulation after comparing a randomly generated number to the expected live percentage. Percent live of remaining cells was then calculated.

Sample Selection

Patient samples were accessed through the University of Virginia Biorepository and Tissue Research Facility. These samples were selected from patients with a definitive diagnosis of node-negative breast cancer and who received no treatment prior to tumor resection. Samples were de-identified before use. All procedures performed in studies involving human participants were in accordance with the ethical standards of the institutional review board of the University of Virginia and with the 1964 Helsinki declaration and its later amendments or comparable ethical standards.

Immunohistochemistry

Formalin-fixed, paraffin-embedded sections were deparaffinized with xylene and rehydrated in graded ethanols and citrate-based antigen retrieval was performed (Vector Labs, Burlingame, CA). Samples were permeabilized (0.01% Triton) and blocked in goat serum. Based on markers previously established in the literature, breast cancer cells were identified by anti-pan-cytokeratin staining and cancer-associated fibroblasts were identified by anti-alpha-smooth muscle actin staining. Samples were incubated with pan-cytokeratin antibody (Thermoscientific) followed by secondary Cy5-goat anti-mouse (Thermoscientific). These steps were then repeated for the TRITC-conjugated alpha-smooth muscle actin antibody (ebioscience). The samples were incubated with DAPI (Sigma-Aldrich, St. Louis, MO) and mounted with Fluoromount-G (SouthernBiotech). All antibodies were used at dilutions recommended by the manufacturer for paraffin-embedded tissues. Stained slides were imaged with an EVOS fluorescent microscope (Ther-

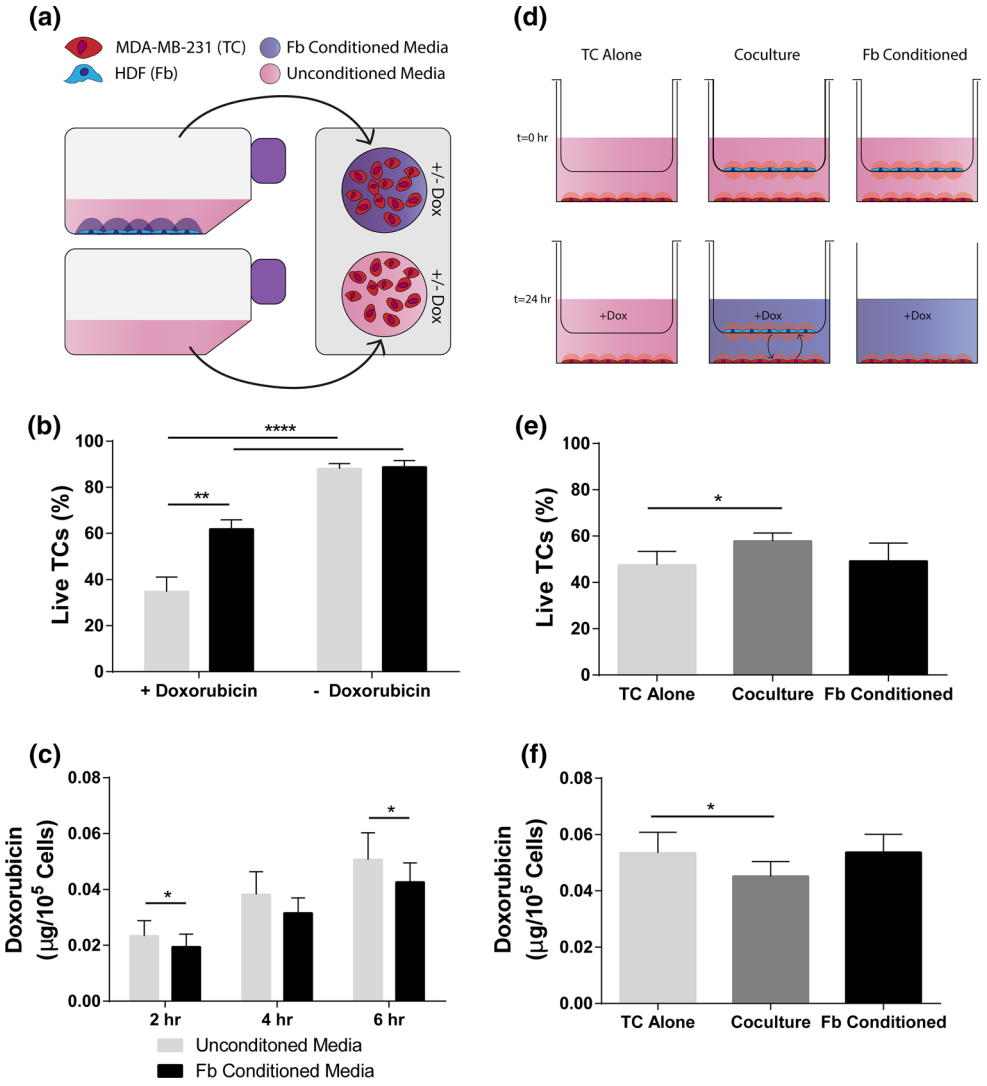

FIGURE 1. Doxorubicin is less cytotoxic to breast cancer cells cultured in fibroblast-conditioned media or co-culture. (a) Schematic of conditioned media experiments: conditioned media is harvested from incubated HDFs (Fbs) after 24 h and applied to MDA-MB-231 breast tumor cells (TCs). (b) Live TCs assessed by nuclear dead stain ± doxorubicin (10 μM) in Fb-conditioned or control media after 24 h as percent of total TCs (n = 5). (c) Cellular uptake of doxorubicin by TCs at successive time points after Doxorubicin (10 μM) application as assessed by fluorescent signal of lysed cells (n = 6). (d) Schematic of insert co-culture experiments: MDA-MB-231 cells (TCs) and HDFs (Fbs) are co-cultured independent of contact for 24 h prior to doxorubicin treatment. In the Fb-conditioned experimental group, the Fbs are removed prior to dosing chemotherapy. (e) Live TCs assessed by nuclear dead stain ± doxorubicin (10 μM) in Fb-conditioned or control media after 24 h as percent of total TCs (n = 5). (f) Cellular uptake of doxorubicin by TCs at 6 h after Doxorubicin (10 μM) application as assessed by fluorescent signal of lysed cells (n = 6). Data are represented as mean ± SEM. *p < 0.05, **p < 0.01, ****p < 0.0001 by paired t-tests (b, e, f) and two-way ANOVA followed by post hoc paired t-tests (c).

moscientific). Random non-overlapping 856 × 476 μm (407, 465 μm^2) regions at the tumor-stroma border were selected for imaging. Images were processed using ImageJ and Photoshop.

Statistical Analysis

Statistical analyses were run using Graphpad Prism. Paired *t*-tests and two-way ANOVA were used for analysis of same subject groups. Unpaired *t*-tests and two-way ANOVA were used for analysis of independent experimental groups and computational data. MANOVA analysis using the SPSS software package was utilized for normalized distance comparisons within experimental gels for both computational and experimental conditions. All assays were performed with a minimum of three biological replicates. $p < 0.05$ was considered statistically significant for all statistical tests.

RESULTS

Fibroblasts Reduce Cancer Cell Death in Response to Doxorubicin and Lowered Levels of Doxorubicin Accumulation

The effects of contact independent fibroblast signaling on cancer cell response to doxorubicin were first tested by treating MDA-MB-231 cells with either HDF conditioned media or comparable control media (Fig. 1a) in 2D for 24 h. Following subsequent doxorubicin treatment for 6 h, tumor cells grown in conditioned media had a greater percentage of live cells compared to unconditioned controls (Fig. 1b). Tumor cells treated with either Fb-conditioned or unconditioned media showed no difference in percent live tumor cells in the absence of doxorubicin. Notably, at 2 and 6 h, the mass of doxorubicin present in cell lysate was significantly decreased following pre-incubation with Fb-conditioned media prior to treatment compared to unconditioned controls (Fig. 1c).

To further test contact independent fibroblast signaling, fibroblasts were seeded on a hanging porous insert with tumor cells seeded onto the bottom of the well plate at a ratio of 4:1 tumor cells to fibroblasts (Fig. 1d). While preconditioning with fibroblasts showed no effect, co-culturing with fibroblasts during treatment yielded a significant increase in the percentage of live tumor cells compared to controls (Fig. 1e). The co-culture condition yielded a decrease in cancer cell-internalized mass of doxorubicin compared to the tumor cells alone control (Fig. 1f). However, there was no difference in doxorubicin accumulation in the conditioned group as compared to the tumor cells alone. Examination of the fibroblasts also revealed that the co-culture condition not only led to changes in the tumor cell population, but also led to opposite effects in fibroblasts. Co-culture led to increased death of fibroblasts and increased uptake of doxorubicin by fibroblasts (Fig. S3).

Cancer Cell Response to Doxorubicin is Dependent on the Ratio of Tumor Cells to Fibroblasts

The tumor border includes a transition from the tumor bulk, with relatively few fibroblasts, to the surrounding stroma, with very few tumor cells. Therefore, it was desirable to determine the extent of the fibroblast protective effect within the context of varied cancer cell to fibroblast ratios and varied total cell densities, of relevance to the tumor-stroma transition (TST) zone.

We selected a range of ratios of tumor cells:fibroblasts (TC:Fb) from 4:1 to 1:4 and created 2D co-cultures in single wells prior to introduction of doxorubicin (Fig. 2a). The total cell number was held constant, and ratios of cells were varied internally. For control comparison, tumor cells were seeded at the same number as the co-culture condition in the absence of fibroblasts. For MDA-MB-231, the percentage of live tumor cells increased linearly with an increase in the seeding number of tumor cells in co-culture with fibroblasts (Fig. 2b and Fig. S4) until higher ratios were reached (16:1) at which point the effect was lost and viability levels matched those of tumor cell alone controls (Fig. 2c). Similar trends were seen for the triple negative line HCC38 (Fig. 2d and the ER+/PR+ line MCF7 (Fig. 2e). Co-cultures at 1:4 TC:Fb showed non-statistically different cell survival compared cancer cells alone for triple negative cell lines (Figs. 2b and 2d), while a ratio of 4:1 yielded the greatest percent live for all cell lines. No difference was observed in the viability of the single cultured tumor cells with regards to the seeding number in response to doxorubicin; however, MCF7 was more sensitive to doxorubicin overall compared to the two triple negative cell lines (Fig. 2e). MCF7 showed reduced response to doxorubicin even at the lowest ratios of TC:Fb, indicating that it is protected by fibroblasts in general and less sensitive to the cellular ratio. Overall and for all cell lines, a decreased response to doxorubicin was associated with a lower ratio of TC:Fb.

To further probe this phenomenon, the number of tumor cells was held constant, and the cell ratio was altered by adjusting only the total number of fibroblasts in co-culture (Fig. S5A), prior to doxorubicin treatment. A control group was also established by seeding tumor cells at the same number as all other experimental conditions without the addition of fibroblasts. A comparable viability effect was observed as seen in the hanging well cultures: A ratio of 4:1 tumor cells to fibroblasts yielded the greatest viability of tumor cells and the greatest difference in viability as compared to the control condition (Fig. S5B). These data indicate that the fibroblast protective effect is not dependent on the total number of tumor cells; rather, it depends on the ratio of tumor cells to fibroblasts. Additionally, while fibroblast-derived factors need to be present to observe the effect, the ratio of tumor cells to fibroblasts, not the total number of fibroblasts, is the determining factor.

Ratiometric Effects are Conserved When Cells are Cultured in a Breast-Mimetic 3D Microenvironment

Since the *in vivo* microenvironment is a three-dimensional space with which the cells can readily interact, and it has been shown that dimensionality can affect therapeutic outcomes in cancer, comparable *in vitro* hydrogel doxorubicin treatment experiments were developed to extend the co-culture experimental

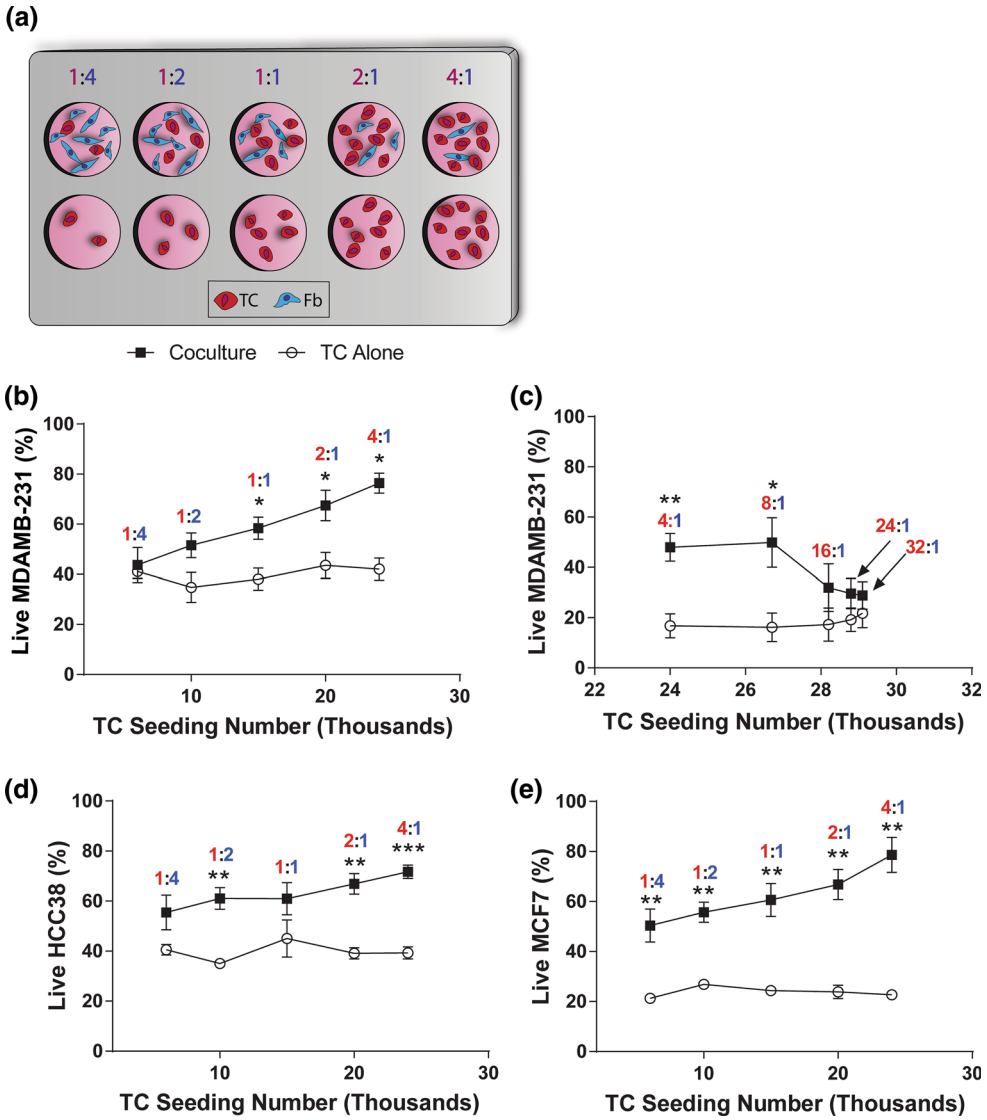

FIGURE 2. In single co-culture, the ratio of tumor cells to fibroblasts alters the viability of tumor cells in response to doxorubicin treatment. (a) Schematic of constant total cell seeding density experiment: TCs (red) and Fbs (blue) were seeded in a culture dish with the total number of cells (TCs + Fbs) held constant. Single cultured TCs were seeded at the same TC density as experimental conditions with no fibroblasts in 2D co-culture. (b) Percent live MDA-MB-231 at low ratios. (c) MDA-MB-231 at high ratios, (d) HCC38, and (e) MCF7 TCs assessed by nuclear dead stain ± doxorubicin (10 μM) after Doxorubicin treatment for 6 h with increasing ratios of TC:Fb (n = 5). Data are represented as mean ± SEM. *p < 0.05, **p < 0.01, ***p < 0.001 by post hoc unpaired t-tests following two-way ANOVA.

findings. Collagen hydrogels were developed with varying ratios of tumor cells and fibroblasts found to be relevant (4:1, 1:1, 1:4) in 2D (Fig. 3a). Control gels were seeded with tumor cells, alone, at the same total cell number as the co-culture hydrogels (Fig. 3b). After treatment was applied by *via* pressure-driven flow, total tumor cell viability in the absence of doxorubicin was approximately 90% for all conditions (Fig. 3c). Analysis of the total tumor cell viability within the gels after treatment indicated that a ratio of 4:1 tumor cells to fibroblasts yielded a significantly higher viability than the comparable single culture condition.

Gradients of Chemotherapy Form Across Invading Edges of Tumors

In addition to the cellular heterogeneity at the tumor edge, increased fluid pressure at the tumor border drives interstitial fluid flow into the adjacent stroma generating a gradient of chemotherapeutic.[32] Collagen hydrogels have been utilized in the past to mimic this region. Here, we developed *in silico* theoretical concentration profiles within collagen hydrogel mimetics based on the geometry of the hydrogels, Darcy's law of fluid transport, and the general diffu-

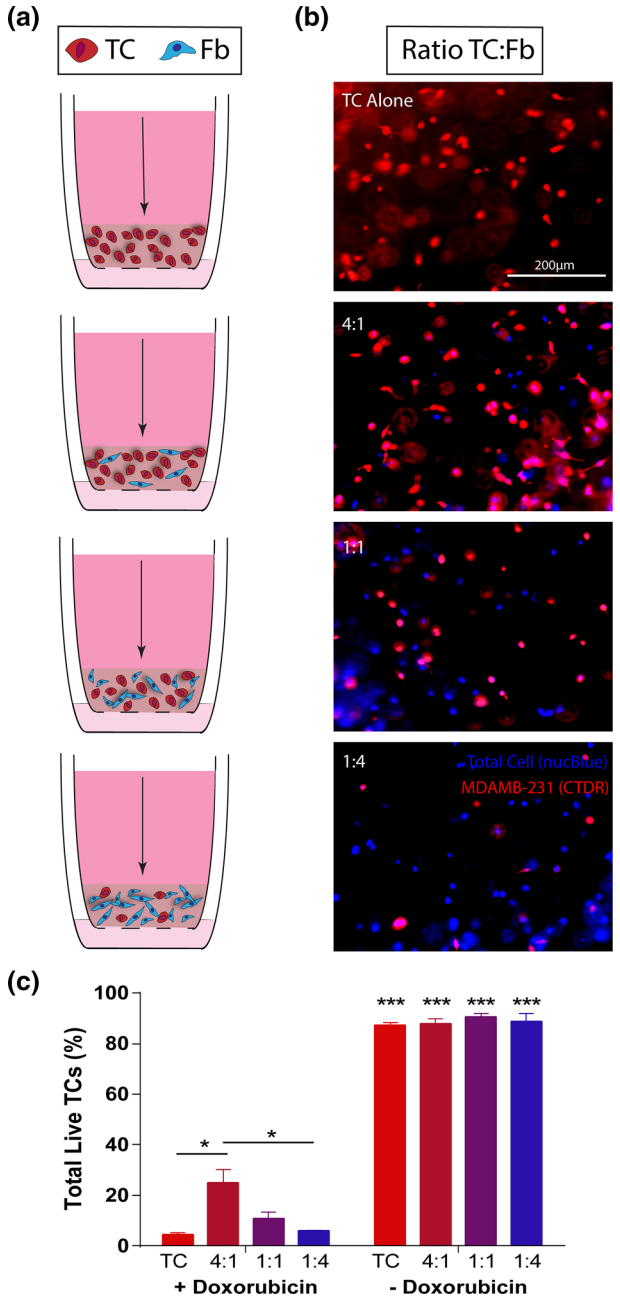

FIGURE 3. Ratiometric response of tumor cells occurs when cells are co-cultured in a breast-mimetic collagen I matrix. (a) Schematic of independent tissue culture insert set-ups for increasing ratios of TCs:Fbs in a collagen I matrix. Arrow indicates direction of application of doxorubicin for 18 h. (b) Fluorescent images of Celltracker deep red-labeled MDA-MB-231(red, TCs) and total cell nuclei (blue, NucBlue) in 3D collagen hydrogels prior to doxorubicin treatment. Cells were seeded at varied ratios with overall cellular concentration held constant (1E6 cells/mL). Blue label without red indicates a fibroblast. (c) Live TCs assessed by nuclear dead stain within collagen gels ± doxorubicin (10 μM) after 18 h application *via* interstitial flow (n = 3). Data are represented as mean ± SEM. *p < 0.01, ***p < 0.001 by post hoc unpaired t-tests following two-way ANOVA analysis. ***Signifies statistical significance to matched + doxorubicin condition.

sion equation (Table 1; Supplemental Methods). Because the fluid velocity is very low (~0.5 um/s), concentration gradients develop between the top and the bottom of the gel (Figs. 4a and S6). Notably, the concentration of the drug was greatest at the top of the gel relative to the bottom. However, it should be noted that the concentration reached steady state in the hydrogel after 5.8 h of simulated flow (Fig. S6).

High Tumor Cell to Fibroblasts Ratios Reduce Cancer Cell Response in an Agent-Based Model of the Tumor Microenvironment

An agent-based *in silico* model (ABM) was developed using the concentration profiles determined in COMSOL, to represent flow mediated doxorubicin treatment through homogenously seeded hydrogels at varied cancer cell to fibroblast ratios (Figs. S1 and S2). Predictive equations for the percentage of live tumor cells were determined from the 2D results (Table 2; Fig. S7). Simulations of 18-h doxorubicin treatment delivered *via* top-to-bottom interstitial flow indicated an increase in overall percentage of live tumor cells in co-culture conditions relative to the tumor cells alone condition (Fig. 4c), and this percentage was greater with increasing ratios of tumor cells to fibroblasts.

The ABM was further utilized to probe spatial variations in cancer cell survival through homogenously seeded hydrogels with different tumor cell:fibroblast ratios. At each depth in the gel, greater ratios of tumor cells to fibroblasts yielded a greater percentage of live tumor cells relative to successively lower ratios (Fig. 4d). All conditions yielded significantly greater viability than the tumor cell alone control condition. Interestingly, for samples with higher ratios, tumor cells at the top of the gel had a significantly lower percent survival as compared to the bottom of the gel due to drug concentration profiles. Our ABM predicted more significant results than our 3D hydrogel experiments, however, the viability trend was comparable between *in vitro* and *in silico* models. Viability of tumor cells in each co-cultured condition was approximately half of the ABM predicted viability percentage. This is likely due to a reduction in the fibroblast protective effect within 3D systems, as compared to 2D culture system, as a result of the extracellular matrix components and greater dispersal of cells.

Development of an In Silico Tumor to Stromal Transition (TST) Model ABM Shows Response Across the Invasive Edge of Tumors

Following confirmation of the fibroblast protective effect in 3D, an *in silico* ABM tumor to stroma tran-

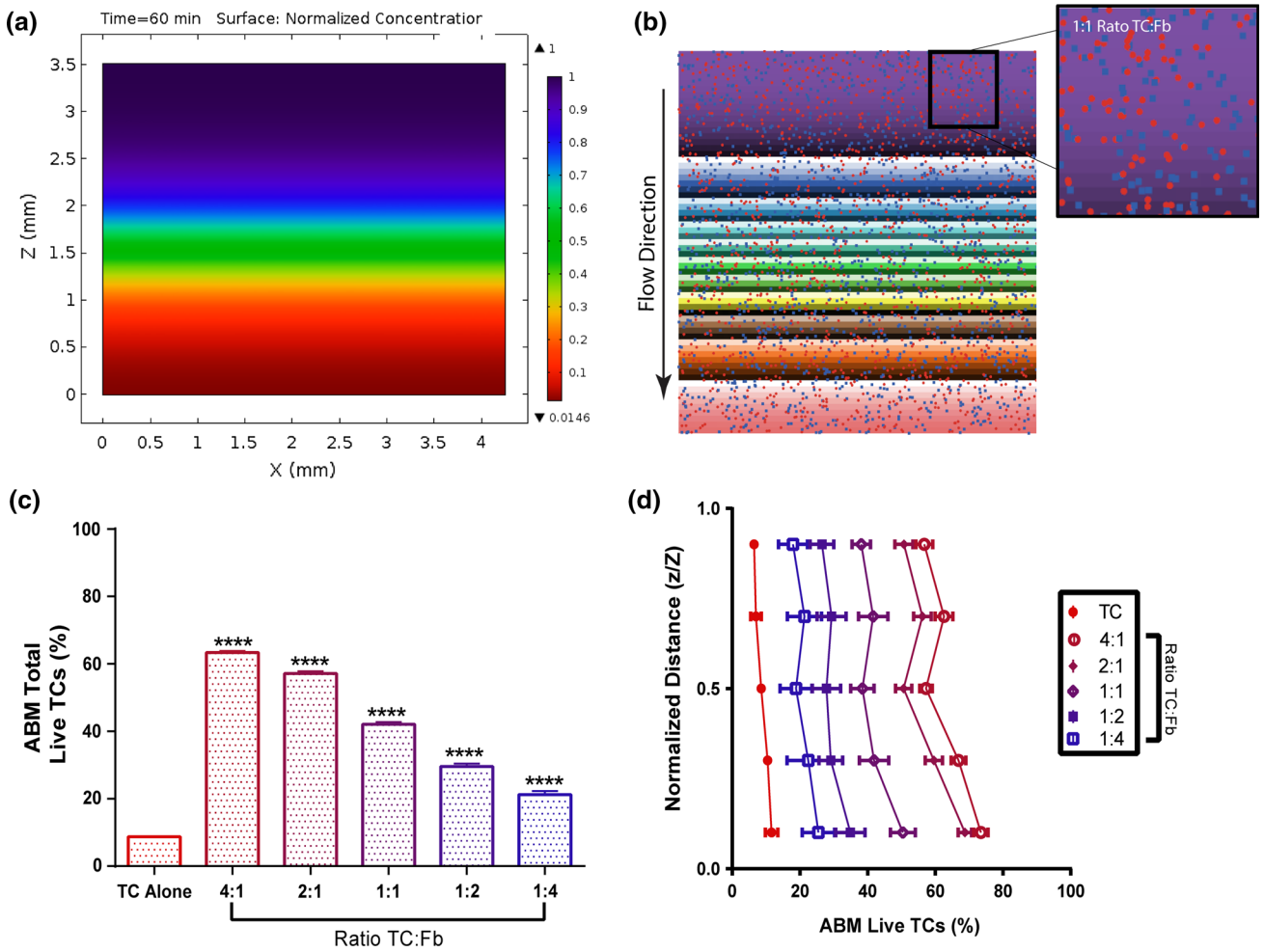

FIGURE 4. Agent-based model (ABM) predicts overall and distance-dependent response of tumor cells to doxorubicin in the 3D collagen hydrogel system. (a) Diffusion-convection concentration gradient developed in Comsol within a simulated 3D hydrogel. Scale gives normalized concentration (C/C_{max}). (b) The agent-based model incorporates concentration profiles, cancer cells, and fibroblasts for *in silico* drug screening. (c) ABM-predicted overall viability for homogenous gels of varied tumor cell:fibroblast ratios (n = 20). (d) Location dependent viability of tumor cells in homogenous gels seeded at varied tumor cell:fibroblast ratios (n = 20). Data are represented as mean ± SEM. ****p < 0.0001 compared to 231 control by post hoc unpaired t-tests following two-way ANOVA analysis. (d) post hoc t-tests after MANOVA analysis which shows significant effects (p < 0.001) for ratios and distance

sition (TST) model (Fig. S1B; Supplemental Movie 1), representing the *in vivo* tumor bulk to stroma transition area (Fig. 5a), was utilized to predict the region specific effects of doxorubicin treatment within a heterogeneous 3D-hydrogel breast mimetic system. For tumor cell alone simulations, the tumor cells in each successive layer within the simulated hydrogel correspond to the number of tumor cells in the comparable layer in the co-culture simulation (Fig. S1C).

Results predicted that tumor cells alone, region specific, cell viability followed the same trend as homogenously seeded tumor cell alone simulations (Fig. 5b), where cancer cell populations that encountered a higher concentration of drug for the longest period of time (top of the gel) had significantly lower viability compared to cell populations at the bottom of the hydrogel, that encountered a lower average concentration of drug. Interestingly, this trend was reversed for co-culture simulations. Tumor cells at the top of the hydrogel, representative of the tumor bulk region, had a greater percentage of live tumor cells as compared to the cancer cell populations at the bottom of the gel, representative of the tumor stromal region. The simulations indicated that tumor cells in the tumor bulk are protected from doxorubicin chemotherapy to a greater extent than tumor cells in the simulated stroma, indicating the potential for a resistant subpopulation within the tumor microenvironment.

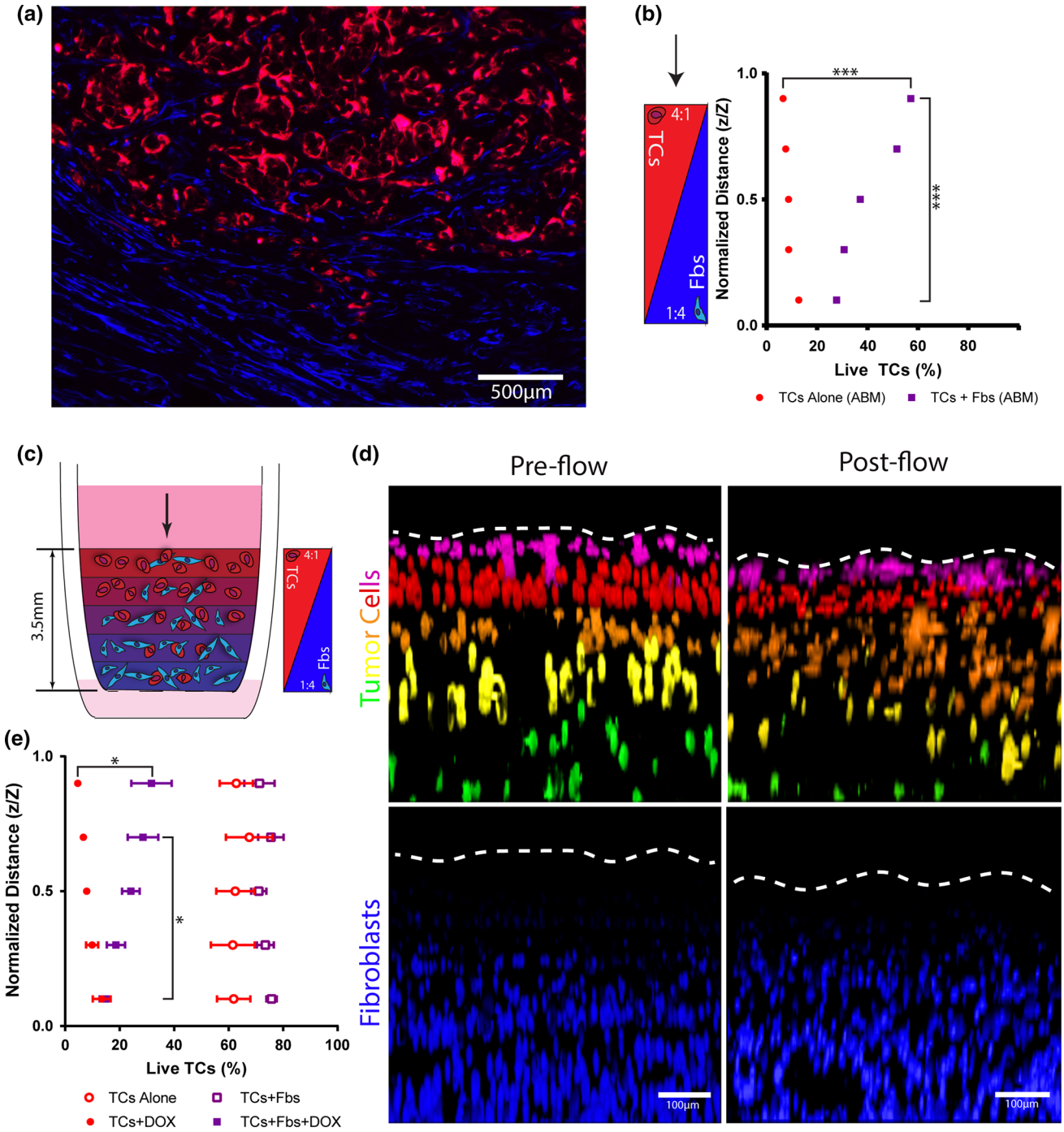

FIGURE 5. Layered *in silico* and *in vitro* models of the tumor to stroma transition zone indicate that tumor cells in the bulk are more viable after doxorubicin than those in the stroma. (a) Tumor-stroma interface from a resected patient breast carcinoma showing tumor cells (pan-cytokeratins, red) and fibroblasts (alpha-smooth muscle actin, blue). (b) ABM predicted percent viability in varied depths within a layered hydrogel with counter-correlated gradients of TCs and Fbs after 18 h of simulated drug treatment ($n = 20$). (c) Schematic of a penta-layered collagen hydrogel setup in a tissue culture insert with countercorrelated gradients of TCs and Fbs to model the tumor to stroma transition zone (TST model). (d) Confocal images of the TST model under control (no treatment) condition prior to (left) and after (right flow) with tumor cells (false colored—top) and fibroblasts (bottom). The tumor cells are labelled with alternating cell tracker dyes (green and deep red) to distinguish each layer. Dotted line indicates top of gel. (e) Live TCs assessed by nuclear dead stain within collagen gels ± doxorubicin (10 μM) and ± fibroblasts at varied depths within the hydrogel for 18 h of treatment. ($n = 3$) Data are represented as mean ± SEM. *$p < 0.05$, ***$p < 0.001$ by *t* test after MANOVA analysis showing significance for distance and group.

A corresponding In Vitro Model of the invasive Edge Indicates Similar Region Specific Cancer Cell Response

A penta-layered hydrogel *in vitro* TST model was created by successively depositing hydrogel solutions with increasing cancer cell to fibroblast ratios from bottom to top of a cell culture insert (Fig. 5c). Tumor cells in alternating layers were labelled with different cell tracker dyes (Fig. 5d). Distinct regions were confirmed, *via* confocal imaging, prior to introduction of flow. These regions were confirmed following flow application (Fig. 5d).

The region-specific viability within the *in vitro* TST model confirmed the trends predicted by the comparable ABM (Fig. 5e), with the addition of fibroblasts increasing viability overall. However, fibroblasts did not confer significantly increased viability in the lowest layer of the TST model as was predicted by the ABM. Tumor cells alone with flow-applied doxorubicin treatment yielded regions at the top of the gel with significantly decreased percentages of live tumor cells as compared to the bottom the hydrogel. By contrast, co-culture (TCs + Fbs) hydrogels yielded significantly greater cancer cell viability at the top of the gel as compared to the bottom of the gel. In the absence of doxorubicin, there was no difference in region specific viability for co-cultured and tumor cell alone TST models.

The Interaction of Transport Properties with Cellular Interactions in the ABM Shows the Importance of Tissue-Level Changes in Cancer Cell Response to Chemotherapy

MCF7 and HCC38 2D viability data was utilized to predict the region specific and overall viability in simulated layered 3D hydrogels with flow (Fig. 6a and 6b). Overall, predicted viability was higher at the top of the gel as compared to the bottom, which is comparable to results observed with MDA-MB-231 cancer cells. Interestingly, however, the difference between predicted viability at the top and bottom of the simulated hydrogel was much less for the MCF7 condition than the other two cell lines. This could indicate a more homogenous treatment response for this cell line. Overall viability was higher for MDA-MB-231 cells than the other cell lines.

Sensitivity analyses of COMSOL parameters emphasize the effects of transport properties on region specific and average cancer cell viability (Fig. 6c). Diffusion alone, in the absence of convection, was not a major mediator of cancer cell death, as drug does not penetrate into the gel after 18 h (Fig. S6). Transport from the bottom of the gel to the top, simulating flow from the stroma to the tumor, yielded an even greater difference in the viability of the cells at the top relative to the bottom of the gel, which yielded a corresponding overall increase in cancer cell viability as compared to the normal flow control (Fig. 6d).

Altering the diffusion coefficient, analogous to changing the size of the drug, while maintaining convective parameters, yielded no significant difference in the general region specific viability of tumor cells (Fig. 6e), except for a 100-fold increase in the diffusion coefficient. Similarly, overall percent live tumor cells within the hydrogels was only significantly altered from the control condition in the case of 100-fold increase in the diffusion coefficient (Fig. 6f). Analysis of the concentration profiles indicated that convection was dominating diffusion (P_e = 2.75–2750) except in the 100-fold context (Fig. S8).

Alterations of the permeability coefficient, analogous to altering the matrix density, and associated alterations in velocity (Fig. S8), while maintaining the diffusion parameters, yielded varied alterations in region specific and overall cancer cell viability (Fig. 6g). While the viability at the top of the gels was always greater than the bottom of the gel, for comparable conditions, increasing the permeability decreased the overall viability (Fig. 6h). At low values of permeability (0.01 and 0.1 K) there was no difference in region specific or overall viability, however, the viability was not zero. This was due to the fact that the gel becomes saturated with drug almost instantly at these values; therefore, the viability effects become dominated by the drug dosage and the fibroblast protective effect. At very low values of permeability, the region specific and overall viability was comparable to diffusion only conditions, indicating that diffusion was dominating convection in these conditions (P_e = 0.275–2.75).

DISCUSSION AND CONCLUSION

Mechanisms Behind Fibroblast Induced Chemotherapy Resistance

Multidrug resistance in cancers is a documented phenomenon, and can be meditated by several cellular mechanisms; however, anthracycline resistance is dominated primarily by classical multidrug resistance.[16] Classical multidrug resistance is described by acquired resistance to chemotherapy by lowered intracellular drug concentration.[68] Shen and colleagues describe the uptake and efflux of doxorubicin within wildtype and multidrug resistant MDA-MB-435 cells and indicate that multidrug resistance in breast cancer cell lines is dominated by increased drug efflux.[58] We believe that the decrease in cancer cell doxorubicin concentration and comparable increase in the per-

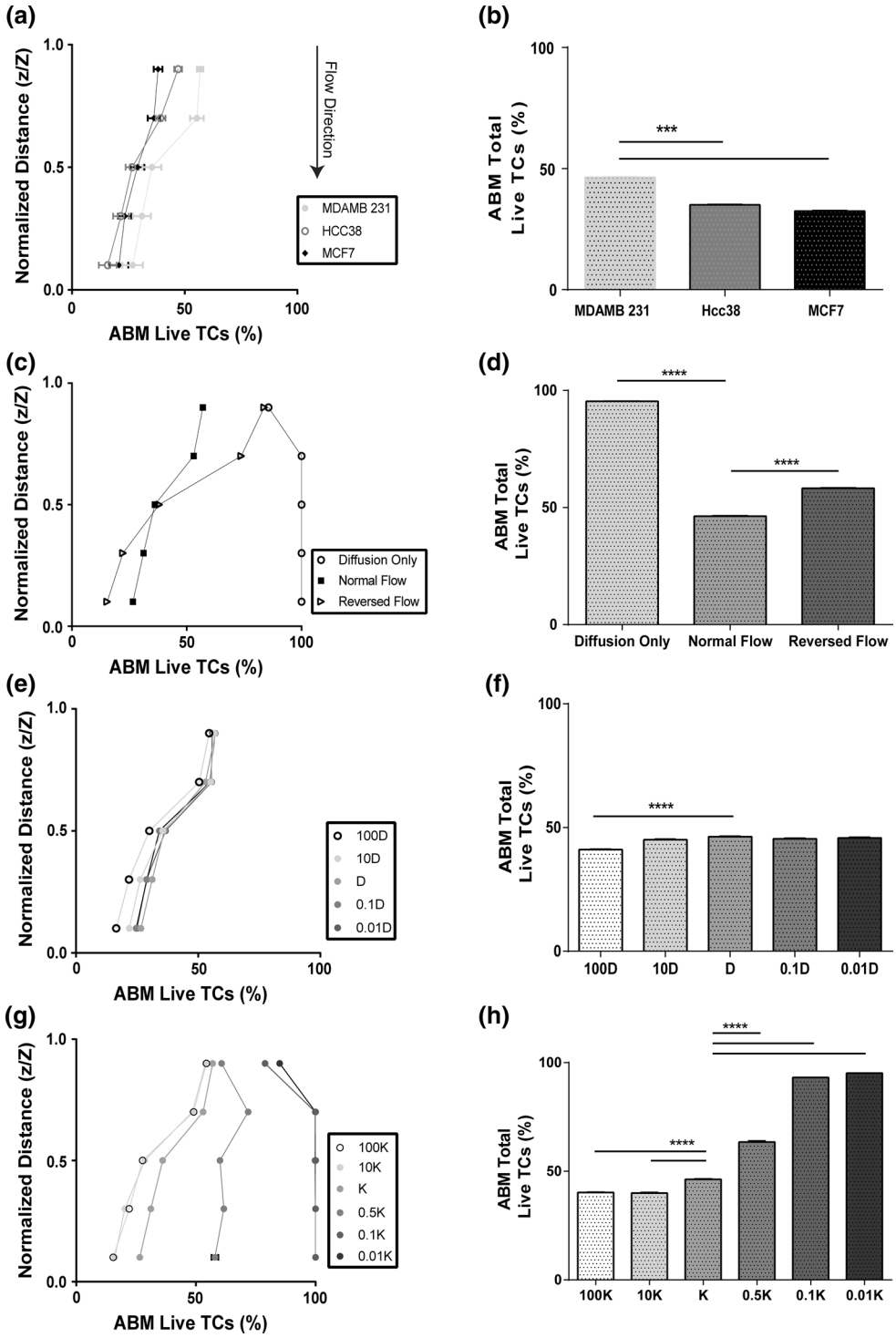

FIGURE 6. The agent-based model reveals complex interactions between cellular response to chemotherapy across the TST zone and transport properties. Cancer cell viability at increasing depth through the agent-based TST model for varied (a) tumor cell type (c) transport conditions including normal flow (top to bottom), reversed flow (bottom to top) and no flow (diffusion only) (e) diffusion coefficients, and (g) permeability coefficients, after 18 h of simulated treatment with 10 μM doxorubicin. (n = 20) Total cancer cell viability within the agent-based TST model for varied (b) tumor cell type (d) transport conditions, (f) diffusion coefficients, and (H) permeability coefficients, after 18 h of simulated treatment with 10 μM doxorubicin. D indicates baseline diffusion coefficient value (6 e^{-11} [m^2/s]), and K represents baseline permeability coefficient value (3.19 e^{-14} [m^2]) (n = 20). Data are represented as mean ± SEM. ****p < 0.0001 by post hoc unpaired t-test following MANOVA (A,C,E,G) and by post hoc unpaired t-tests following two-way ANOVA analysis (b, d, f, h). All main effects were significant by MANOVA or ANOVA.

centage of live tumor cells may be due to classical drug resistance, mediated by drug efflux. Additionally, fibroblast doxorubicin accumulation in the co-culture condition was not negligible, however, the concentration of extracellular doxorubicin after 6 h (~8 μM) was still above the determined IC50 (3.7 μM) for MDA-MB-231 cells. Two studies have found that both the cytoplasm and the nucleus of MDA breast tumor cells become saturated prior to 6 h at varied doses of doxorubicin,[58,72] and this saturation occurs even at a dosed doxorubicin concentration as low as 5 μM.[58] Therefore, it is not likely that the reduced viability in co-culture conditions is simply due to uptake by stromal fibroblasts, as indicated by previous literature. However, localized effects of this accumulation could have enhanced effects on total tumor treatment response based on observations of gradient formation of doxorubicin in patients and correlating with resistance to treatment.[32]

From our data, we interpret that a concentration-dependent, fibroblast-derived signaling molecule is necessary for the protective effect to occur, and this effect is observed at higher ratios of tumor cells to fibroblasts, regardless of the overall cell numbers. Fibroblast activation, a major hallmark of cancer-associated fibroblasts, has been attributed to TGFβ, reactive oxygen species, extracellular matrix modifications, and interstitial fluid flow,[61] among other mechanisms. Activation of fibroblasts leads to further secretion of TGFβ, secretion of other cytokines such as IL-6, and extracellular matrix molecules such as Tenascin C.[29] TGFβ and IL-6 both increase resistance to anthracycline chemotherapy in breast cancer,[1,5] and Tenascin C is associated with chemoresistance in lung cancer.[55] It's possible that, in our system, the ratiometric effect is due to a unique balance between signaling molecules from cancer cells to fibroblasts on a per cell basis needing to be higher than signaling molecules from fibroblasts to cancer cells, but the effect is amplified when cells are touching, sharing an extracellular matrix, or subjected to flow as in our co-culture systems. Fibroblasts have also been associated with creating niches in which cancer stem cells, a particularly drug resistant population of cancer cells, reside and proliferate.[10] These niches may form naturally within our 3D system, further contributing to increased resistance.

Drug Transport in the Tumor Microenvironment

In addition to stromal signaling, fluid dynamics can alter drug concentration gradients and affect region specific and overall viability trends in the tumor border region.[24,53] Reversed flow enhances the cancer cell viability in the bulk region and simultaneously decreases the viability in the stromal region, while increasing the overall viability.[24] Diffusion alone significantly reduces the effectiveness of the chemotherapy, at 18 h of simulation, due to lack of solute penetration into the hydrogel. These results indicate that convection is a dominant factor for concentration profile development and corresponding cancer viability response.[32] This is further confirmed by alterations of the diffusion coefficient, while simultaneously keeping convection constant. In these simulations, the diffusion coefficient only affects the viability at very large values. This confirms that convection is the driving force for doxorubicin concentration development, and diffusion dominates only when molecules are very small.

These results are comparable to those reported by Jain and colleagues [24–27]; the authors highlight the importance of convection and diffusion for solute transport in neoplastic tissues. Specifically, convection is dominant in these tissues when the molecular weight of the solute is significantly large, while diffusion dominates with very small particles.[28] This rationale was further used to explore the transport effects of large molecules within the tumor interstitium and corresponding implications for antibody-based drug delivery.[26] The results indicate that high molecular weight drug efficacy, in whole tumors, is attenuated by extravasation from the tumor bulk. While doxorubicin would not be considered a large molecule drug, it is well within the size range for convection dominant flow in neoplastic tissues.[24] Other larger molecules, such as immunotherapies, would be further transported by convection and thus subject to increased diffusive transport constraints.

However, convection dominance is also mediated by the permeability of the tissue of interest. As breast tumor heterogeneity affects the permeability and corresponding fluid velocity[23] *in vivo*, characterizations of alterations in permeability were explored to determine the effect of tumor permeability heterogeneity on cancer cell viability. Physiologic breast tumor interstitial fluid velocities are predicted to be between 0-10 μm/s as compared to normal interstitial velocities between 0.1 and 1 μm/s.[19] The permeability sensitivity analysis accounted for velocity alterations within these ranges. Diffusion dominates convection when interstitial velocities are decreased to normal tissue values (0.1 and 0.01 K), as is apparent from comparison to the diffusion alone concentration profile. Similarly, regional viability was comparable between the low permeability and diffusion only conditions. As permeability is increased, viability decreases due to rapid homogenization of concentration gradients. Therefore, decreasing the permeability would decrease the extravasation rate from the tumor bulk and subsequently increase the efficacy of overall drug penetration into the tumor, previously reported as a method to increase whole tumor therapeutic efficacy.[46] However,

regional drug efficacy at the tumor border could be potentially attenuated with decreased permeability, as dispersed concentration profiles would develop in this region.

Interestingly, fibroblasts are major players in altering both permeability and diffusivity of molecules within the tumor microenvironment. Activated fibroblasts deposit ECM and alter matrix alignment in ways that contribute to reduced permeability and diffusivity through the system, thus limiting therapeutic transport.[47] A number of factors contribute to fibroblast activation, but interstitial fluid flow and chemotherapies such as 5-fluorouracil, epirubicin, and cyclophosphamide have been linked specifically to increases in activation and collagen accumulation.[11,38] These cells not only limit the transport of therapies, but also contribute to increases in cancer cell invasion at these border regions, the initiating site of metastatic spread.[62] Our model does not account for these emergent fibroblast behaviors, however, future iterations could incorporate feedback loops to adjust these parameters as they affect transport in the TME.

Implications of Our Models to Therapeutic Efficacy and Clinical Response

Together our data indicate that several TME-specific factors affect cancer cell viability within the tumor stoma transition region. Interestingly, we see that it is the cells nearest the modeled invading stroma that are more susceptible to therapy than those in the tumor bulk. There is a great deal of research focused on targeting or preventing development of invading cells within these stromal zones [18,44,45,66] as a means for preventing metastasis. Examination of tumor cells live *in vivo* indicates heterogeneity in the subsets of cells that invade through tissues.[12] Though it is intuitive to think that invaded cancer cells will not be accessed by therapies and thus will continue to invade and lead to systemic metastases, our data here may indicate that cells closer to the bulk may resist treatment better and potentially become invading cells post-therapeutic administration. This invasion may be enhanced by interstitial fluid flow, a known promoter of cellular invasion in multiple cancers. Though our results are limited by only examining only one fibroblast type, we have identified this ratiometric effect across three breast cancer cell lines. Due to the ubiquitous presence of fibroblasts and increased fluid flow at invasive edges of cancers in multiple organs, our *in silico* and *in vitro* findings may translate in part to other cancers. This is particularly true for highly desmoplastic cancers, such as pancreatic carcinoma, which are known to be highly transport limited with extreme ratios of stroma to cancer compared to other solid tumors.[50,51]

In breast cancer, specifically, high percentages of stroma within the tumor bulk are a poor prognostic indicator in breast cancer patients. These studies have found that patients with high stroma:tumor ratios have worse progression-free survival than those with low[8,41]; however, these studies have defined high and low based on an arbitrary 50% overall ratio, and have not specifically examined nuances in these ratios. In line with this, multiple papers have shown that the removal of fibroblasts or reduction in fibroblast activation aids therapies in mouse models of cancer.[2,36] However, the contribution of regional heterogeneity has not been clinicopathologically studied. Micropatterning and spheroid co-culture models have revealed some evidence that there is regional variability in these effects. Recent studies with Lapatinib indicate that the distance between fibroblasts and cancer cells predicts therapeutic response.[40] There have been no *in vivo* studies examining the intratumor heterogeneity of drug response with spatial resolution. However, classically drug resistant cells, such as cancer stem cells[6] and cells expressing the classical multidrug resistance gene P-glycoprotein, have been identified in invasive regions and metastases of multiple carcinomas, including breast.[22,42,70] Though evidence suggests relevance of the type of spatial heterogeneity in drug response that we observe, further investigation is required to determine how cells *in vivo* are responding to therapies across this tumor border region and determine the implications of both increased interstitial fluid flow and ratiometric stromal heterogeneity for patient outcomes.

CONCLUSION

Here we find that there is a distinctive interaction between the contributions of fibroblasts and transport to the activity of a common chemotherapeutic, doxorubicin, in a simulated breast cancer microenvironment. Our findings indicate that fibroblasts confer poorer therapeutic efficacy of doxorubicin overall, yet, higher ratios of tumor cells to fibroblasts results in increased drug resistance in three cell lines over lower ratios. This may suggest that it is the cells nearer the bulk of the tumor that resist treatment as opposed to those that have already invaded surrounding tissue. For the invasive edge of tumors, modeled here, where interstitial fluid flow is heightened, these protective effects are dominant over transport limitations within. However, modulation of the transport properties in line with interregional heterogeneity in tumors can drastically shift these responses. Our tissue engineered and *in silico* models, based on clinical samples of breast cancer invasive stromal regions, indicate that it is

important to study transport and cellular interactions simultaneously when examining cancer-related therapy, as both factors may play an important, yet variable, role in the *in vivo* response of cancer cells to chemotherapy.

ELECTRONIC SUPPLEMENTARY MATERIAL

The online version of this article (doi:10.1007/s12195-017-0498-3) contains supplementary material, which is available to authorized users.

ACKNOWLEDGMENTS

The researchers would like to acknowledge Lynette Sequeira for her technical laboratory assistance, Charles Calderwood for statistical assistance. We also thank RC Cornelison, RP Pompano, SM Peirce-Cottler, and SS Blemker for helpful discussion. We would also like to acknowledge the Janes Lab at UVa for initial contribution of cell lines, the Advanced Microscopy Facility and the Biorepository and Tissue Research Facility. This research was funded in part through funding to JM Munson from the UVa Cancer Center through the NCI Cancer Center Support Grant P30 CA44579 and support from the Snell Endowment Fund and Commonwealth of VA, the School of Medicine, and funding to GF Beeghly from the Harrison Undergraduate Research Awards Center at UVa.

CONFLICT OF INTEREST

The authors declare that they have no conflicts of interest.

ETHICAL APPROVAL

All human samples were acquired according to the ethical standards. No animal studies were performed in this work.

REFERENCES

[1]Bandyopadhyay, A., *et al.* Doxorubicin in combination with a small TGFβ inhibitor: a potential novel therapy for metastatic breast cancer in mouse models. *PLoS One* 5:10365, 2010.

[2]Brennen, W. N., D. M. Rosen, H. Wang, J. T. Isaacs, and S. R. Denmeade. Targeting carcinoma-associated fibroblasts within the tumor stroma with a fibroblast activation protein-activated prodrug. *JNCI J. Natl. Cancer Inst.* 104:1320–1334, 2012.

[3]Carey, L. A., *et al.* The triple negative paradox: primary tumor chemosensitivity of breast cancer subtypes. *Clin. Cancer Res.* 13(8):2329–2334, 2007.

[4]Chen, A. A., G. H. Underhill, and S. N. Bhatia. Multiplexed, high-throughput analysis of 3D microtissue suspensions. *Integr. Biol.* 2:517, 2010.

[5]Conze, D., *et al.* Autocrine production of interleukin 6 causes multidrug resistance in breast cancer cells. *Cancer Res.* 61(24):8851–8858, 2001.

[6]Dean, M., T. Fojo, and S. Bates. Tumour stem cells and drug resistance. *Nat. Rev. Cancer* 5:275–284, 2005.

[7]Deisboeck, T. S., L. Zhang, J. Yoon, and J. Costa. *In silico* cancer modeling: is it ready for prime time? *Nat. Clin. Pract. Oncol.* 6:34–42, 2009.

[8]Dekker, T. J. A., *et al.* Prognostic significance of the tumor-stroma ratio: validation study in node-negative premenopausal breast cancer patients from the EORTC perioperative chemotherapy (POP) trial (10854). *Breast Cancer Res. Treat.* 139:371–379, 2013.

[9]Falkenberg, N., *et al.* Three-dimensional microtissues essentially contribute to preclinical validations of therapeutic targets in breast cancer. *Cancer Med.* 5:703–710, 2016.

[10]Fang, W. B., M. Yao, and N. Cheng. Priming cancer cells for drug resistance: role of the fibroblast niche. *Front. Biol.* 9:114–126, 2014.

[11]Farmer, P., *et al.* A stroma-related gene signature predicts resistance to neoadjuvant chemotherapy in breast cancer. *Nat. Med.* 15:68–74, 2009.

[12]Friedl, P., and S. Alexander. Cancer invasion and the microenvironment: plasticity and reciprocity. *Cell* 147:992–1009, 2011.

[13]Fukuda, J., *et al.* Micropatterned cell co-cultures using layer-by-layer deposition of extracellular matrix components. *Biomaterials* 27:1479–1486, 2006.

[14]Gao, M.-Q., *et al.* Stromal fibroblasts from the interface zone of human breast carcinomas induce an epithelial-mesenchymal transition-like state in breast cancer cells *in vitro*. *J. Cell Sci.* 123:3507–3514, 2010.

[15]Gattazzo, F., A. Urciuolo, and P. Bonaldo. Extracellular matrix: a dynamic microenvironment for stem cell niche. *Biochim. Biophys. Acta Gen. Subj.* 2506–2519:2014, 1840.

[16]Gottesman, M. M., T. Fojo, and S. E. Bates. Multidrug resistance in cancer: role of ATP-dependent transporters. *Nat. Rev. Cancer* 2:48–58, 2002.

[17]Griffith, L. G., and M. A. Swartz. Capturing complex 3D tissue physiology *in vitro*. *Nat. Rev. Mol. Cell Biol.* 7:211–224, 2006.

[18]Gritsenko, P. G., O. Ilina, and P. Friedl. Interstitial guidance of cancer invasion. *J. Pathol.* 226:185–199, 2012.

[19]Haessler, U., J. C. M. Teo, D. Foretay, P. Renaud, and M. A. Swartz. Migration dynamics of breast cancer cells in a tunable 3D interstitial flow chamber. *Integr. Biol.* 4:401, 2012.

[20]Hazlehurst, L. A., J. S. Damiano, I. Buyuksal, W. J. Pledger, and W. S. Dalton. Adhesion to fibronectin via beta1 integrins regulates p27kip1 levels and contributes to cell adhesion mediated drug resistance (CAM-DR). *Oncogene* 19:4319–4327, 2000.

[21]Heldin, C.-H., K. Rubin, K. Pietras, and A. Ostman. High interstitial fluid pressure—an obstacle in cancer therapy. *Nat. Rev. Cancer* 4:806–813, 2004.

[22]Hennequin, E., C. Delvincourt, C. Pourny, and J. C. Jardillier. Expression of MDR1 gene in human breast primary tumors and metastases. *Breast Cancer Res. Treat.* 26:267–274, 1993.

[23]Huber, S., *et al*. Breast tumors: computer-assisted quantitative assessment with color Doppler US. *Radiology* 192:797–801, 1994.
[24]Jain, R. K. Transport of molecules in the tumor interstitium: a review. *Cancer Res*. 47:3039–3051, 1987.
[25]Jain, R. K. Transport of molecules, particles, and cells in solid tumors. *Annu. Rev. Biomed. Eng*. 1:241–263, 1999.
[26]Jain, R. K., and L. T. Baxter. Mechanisms of heterogeneous distribution of monoclonal antibodies and other macromolecules in tumors: significance of elevated interstitial pressure. *Cancer Res*. 48:7022–7032, 1988.
[27]Jain, R. K., R. T. Tong, and L. L. Munn. Effect of vascular normalization by antiangiogenic therapy on interstitial hypertension, peritumor edema, and lymphatic metastasis: insights from a mathematical model. *Cancer Res*. 67:2729–2735, 2007.
[28]Jang, S. H., M. G. Wientjes, D. Lu, and J. L. S. Au. Drug delivery and transport to solid tumors. *Pharm. Res*. 20:1337–1350, 2003.
[29]Kalluri, R., and M. Zeisberg. Fibroblasts in cancer. *Nat. Rev. Cancer* 6:392–401, 2006.
[30]Kingsmore, K. M., *et al*. Interstitial flow differentially increases patient-derived glioblastoma stem cell invasion via CXCR4, CXCL12, and CD44-mediated mechanisms. *Integr. Biol*. 8(12):1246–1260, 2016.
[31]Knowlton, S., S. Onal, C. H. Yu, J. J. Zhao, and S. Tasoglu. Bioprinting for cancer research. *Trends Biotechnol*. 33:504–513, 2015.
[32]Lankelma, J., *et al*. Doxorubicin gradients in human breast cancer. *Clin. Cancer Res*. 5:1703–1707, 1999.
[33]LeBedis, C., K. Chen, L. Fallavollita, T. Boutros, and P. Brodt. Peripheral lymph node stromal cells can promote growth and tumorigenicity of breast carcinoma cells through the release of IGF-I and EGF. *Int. J. Cancer* 100:2–8, 2002.
[34]Liu, W., *et al*. Magnetically controllable 3D microtissues based on magnetic microcryogels. *Lab Chip* 14:2614, 2014.
[35]Ljungkvist, A. S. E., J. Bussink, P. F. J. W. Rijken, J. H. A. M. Kaanders, A. J. Van der Kogel, and J. Denekamp. Vascular architecture, hypoxia, and proliferation in first-generation xenografts of human head-and-neck squamous cell carcinomas. *Int. J. Radiat. Oncol. Biol. Phys*. 54:215–228, 2002.
[36]Loeffler, M., J. A. Krüger, A. G. Niethammer, and R. A. Reisfeld. Targeting tumor-associated fibroblasts improves cancer chemotherapy by increasing intratumoral drug uptake. *J. Clin. Invest*. 116:1955–1962, 2006.
[37]Loessner, D., K. S. Stok, M. P. Lutolf, D. W. Hutmacher, J. A. Clements, and S. C. Rizzi. Bioengineered 3D platform to explore cell–ECM interactions and drug resistance of epithelial ovarian cancer cells. *Biomaterials* 31:8494–8506, 2010.
[38]Lotti, F., *et al*. Chemotherapy activates cancer-associated fibroblasts to maintain colorectal cancer-initiating cells by IL-17A. *J. Exp. Med*. 210(13):2851–2872, 2013.
[39]Martin, K. S., S. S. Blemker, and S. M. Peirce. Agent-based computational model investigates muscle-specific responses to disuse-induced atrophy. *J. Appl. Physiol*. 118:1299–1309, 2015.
[40]Marusyk, A., *et al*. Spatial proximity to fibroblasts impacts molecular features and therapeutic sensitivity of breast cancer cells influencing clinical outcomes. *Cancer Res*. 76:6495–6506, 2016.
[41]Moorman, A. M., R. Vink, H. J. Heijmans, J. van der Palen, and E. A. Kouwenhoven. The prognostic value of tumour-stroma ratio in triple-negative breast cancer. *Eur. J. Surg. Oncol*. 38:307–313, 2012.
[42]Morrison, B. J., *et al*. Breast cancer stem cells: implications for therapy of breast cancer. *Breast Cancer Res*. 10:210, 2008.
[43]Munson, J. M., and A. C. Shieh. Interstitial fluid flow in cancer: implications for disease progression and treatment. *Cancer Manag. Res*. 6:317–328, 2014.
[44]Munson, J. M., *et al*. Anti-invasive adjuvant therapy with imipramine blue enhances chemotherapeutic efficacy against glioma. *Sci. Transl. Med*. 4:127ra36, 2012.
[45]Munson, J. M., R. V. Bellamkonda, and M. A. Swartz. Interstitial flow in a 3d microenvironment increases glioma invasion by a cxcr4-dependent mechanism. *Cancer Res*. 73:1536–1546, 2013.
[46]Navalitloha, Y., E. S. Schwartz, E. N. Groothuis, C. V. Allen, R. M. Levy, and D. R. Groothuis. Therapeutic implications of tumor interstitial fluid pressure in subcutaneous RG-2 tumors. *Neuro. Oncol*. 8:227–233, 2006.
[47]Netti, P. A., D. A. Berk, M. A. Swartz, A. J. Grodzinsky, and R. K. Jain. Role of extracellular matrix assembly in interstitial transport in solid tumors. *Cancer Res*. 60:2497–2503, 2000.
[48]Olsen, M. M., and H. T. Siegelmann. multiscale agent-based model of tumor angiogenesis. *Procedia Comput. Sci*. 18:1016–1025, 2013.
[49]Pietras, K., and A. Östman. Hallmarks of cancer: Interactions with the tumor stroma. *Exp. Cell Res*. 316:1324–1331, 2010.
[50]Provenzano, P. P., and S. R. Hingorani. Hyaluronan, fluid pressure, and stromal resistance in pancreas cancer. *Br. J. Cancer* 108:1–8, 2013.
[51]Provenzano, P. P., C. Cuevas, A. E. Chang, V. K. Goel, D. D. Von Hoff, and S. R. Hingorani. Enzymatic targeting of the stroma ablates physical barriers to treatment of pancreatic ductal adenocarcinoma. *Cancer Cell* 21:418–429, 2012.
[52]Raghunand, N., *et al*. Enhancement of chemotherapy by manipulation of tumour pH. *Br. J. Cancer* 80:1005–1011, 1999.
[53]Ramanujan, S., A. Pluen, T. D. McKee, E. B. Brown, Y. Boucher, and R. K. Jain. Diffusion and convection in collagen gels: implications for transport in the tumor interstitium. *Biophys. J*. 83:1650–1660, 2002.
[54]Rouzier, R., *et al*. Breast cancer molecular subtypes respond differently to preoperative chemotherapy. *Clin. Cancer Res*. 11(16):5678–5685, 2005.
[55]Sethi, T., *et al*. Extracellular matrix proteins protect small cell lung cancer cells against apoptosis: a mechanism for small cell lung cancer growth and drug resistance *in vivo*. *Nat. Med*. 5:662–668, 1999.
[56]Shain, K. H., and W. S. Dalton. Cell adhesion is a key determinant in de novo multidrug resistance (MDR): new targets for the prevention of acquired MDR. *Mol. Cancer Ther*. 1:69–78, 2001.
[57]Shannon, A. M., D. J. Bouchier-Hayes, C. M. Condron, and D. Toomey. Tumour hypoxia, chemotherapeutic resistance and hypoxia-related therapies. *Cancer Treat. Rev*. 29:297–307, 2003.
[58]Shen, F., *et al*. Quantitation of doxorubicin uptake, efflux, and modulation of multidrug resistance (MDR) in MDR human cancer cells. *J. Pharmacol. Exp. Ther*. 324:95–102, 2008.
[59]Shen, K., *et al*. Resolving cancer–stroma interfacial signalling and interventions with micropatterned tumour–stromal assays. *Nat. Commun*. 5:5662, 2014.

[60]Shieh, A. C. Biomechanical forces shape the tumor microenvironment. *Ann. Biomed. Eng*. 39:1379–1389, 2011.
[61]Shieh, A. C., H. A. Rozansky, B. Hinz, and M. A. Swartz. Tumor cell invasion is promoted by interstitial flow-induced matrix priming by stromal fibroblasts. *Cancer Res*. 71:790–800, 2011.
[62]Shieh, A. C., H. A. Rozansky, B. Hinz, and M. A. Swartz. Tumor cell invasion is promoted by interstitial flow-induced matrix priming by stromal fibroblasts. *Cancer Res*. 71:790–800, 2011.
[63]Shields, J. D., M. E. Fleury, C. Yong, A. A. Tomei, G. J. Randolph, and M. A. Swartz. Autologous chemotaxis as a mechanism of tumor cell homing to lymphatics via interstitial flow and autocrine CCR7 signaling. *Cancer Cell* 11:526–538, 2007.
[64]Subik, K., *et al*. The expression patterns of ER, PR, HER2, CK5/6, EGFR, Ki-67 and AR by immunohistochemical analysis in breast cancer cell lines. *Breast Cancer (Auckl.)* 4:35–41, 2010.
[65]Tasoglu, S., and U. Demirci. Bioprinting for stem cell research. *Trends Biotechnol*. 31:10–19, 2013.
[66]Tchou, J., and J. Conejo-Garcia. Targeting the tumor stroma as a novel treatment strategy for breast cancer: shifting from the neoplastic cell-centric to a stroma-centric paradigm. *Adv. Pharmacol*. 65:45–61, 2012.
[67]Trédan, O., C. M. Galmarini, K. Patel, and I. F. Tannock. Drug resistance and the solid tumor microenvironment. *JNCI J. Natl. Cancer Inst*. 99:1441–1454, 2007.
[68]Ueda, K., C. Cardarelli, M. M. Gottesman, and I. Pastan. Expression of a full-length cDNA for the human "MDR1" gene confers resistance to colchicine, doxorubicin, and vinblastine. *Proc. Natl. Acad. Sci. USA* 84:3004–3008, 1987.
[69]Walpole, J., J. C. Chappell, J. G. Cluceru, F. Mac Gabhann, V. L. Bautch, and S. M. Peirce. Agent-based model of angiogenesis simulates capillary sprout initiation in multicellular networks. *Integr. Biol. (Camb.)* 7:987–997, 2015.
[70]Weinstein, R. S., *et al*. Relationship of the expression of the multidrug resistance gene product (P-glycoprotein) in human colon carcinoma to local tumor aggressiveness and lymph node metastasis. *Cancer Res*. 51:2720–2726, 1991.
[71]Whiteside, T. L. The tumor microenvironment and its role in promoting tumor growth. *Oncogene* 27:5904–5912, 2008.
[72]Wong, H. L., R. Bendayan, A. M. Rauth, H. Y. Xue, and K. Babakhanian. A mechanistic study of enhanced doxorubicin uptake and retention in multidrug resistant breast cancer cells using a polymer-lipid hybrid nanoparticle system. *J. Pharmacol. Exp. Ther*. 317:1372–1381, 2006.
[73]Zhang, L., C. G. Strouthos, Z. Wang, and T. S. Deisboeck. Simulating brain tumor heterogeneity with a multiscale agent-based model: linking molecular signatures, phenotypes and expansion rate. *Math. Comput. Model*. 49:307–319, 2009.
[74]Zhang, L., Z. Wang, J. A. Sagotsky, and T. S. Deisboeck. Multiscale agent-based cancer modeling. *J. Math. Biol*. 58:545–559, 2009.
[75]Zhao, Y., *et al*. Three-dimensional printing of Hela cells for cervical tumor model *in vitro*. *Biofabrication* 6:35001, 2014.